Chapter 4

Local shower age and segmented slope parameters

4.1 Introduction

The Earth's atmosphere is hit constantly by CRs from different galactic and extragalactic sources. Ground based detector arrays are designed for the measurement of their composition and energy spectrum by detecting the secondary particles of the EASs induced by the CR particles. Electrons ($\mathrm{e}^- + \mathrm{e}^+$) and muons ($\mu^- + \mu^+$) in the EAS constitute the major contribution to the ground detector signals. Densities of these particles at various detector locations from the EAS core are then obtained from the analysis of detector signals. In an EAS experiment, the electron and muon densities, and their arrival times, are known to be the chief observables to extract any information of the primary CRs.

The modeling of LDD of EAS particles through MC simulations is needed in any experiment in order to interpret the data. By applying the shower reconstruction to the simulated and observed LDD data of electrons independently exploiting a suitable LDF, the important shower parameters namely the shower/electron size (N_e), the EAS core and the s are obtained. Some earlier observations (e.g. in [1]) and recent simulation studies indicate that the LDD of shower electrons could not be described with a single age, instead in terms of local ages ($\mathrm{s}^{\mathrm{electron}}_{\mathrm{local}}(\mathrm{r})$) at different radial bands from the EAS core location [2, 3]. In recent past, we have observed that the nature of variation of the local age with radial distance maintains nearly the same configuration independent of the primary CR energies.

The above study indicates that the local age as a function of the radial distance from the EAS core exhibits some sort of scaling nature.

In this work, we have extended the concept of the scaling nature of LDD of electrons in terms of the local age parameter (LAP i.e. $s_{\rm local}^{\rm electron}(r)$) in earlier works to LDD of muons by exploiting simulation data from a MC CR shower generator *CORSIKA* [22]. In order to substantiate the predictions by the simulation, we also examine the possibility of utilizing experimental LDD data of electrons and muons from KASCADE experiment for the purpose of comparison and interpretation.

Several air shower groups have proposed different profile functions to describe the lateral distribution of muons from the EAS core, in analogy to the LDFs for electrons. The LDFs of hadron induced showers were basically constructed empirically or seeded from the electromagnetic cascade theory. Here, we choose the well known NKG function for estimating the LAP from LDD data of electrons and muons independently. For estimating the segmented (or local) slope parameters (SSP i.e. $\beta_{\rm ss}^{\rm muon}(r)$) from LDD of muons, the so called Greisen structure function has been used. The NKG type LDF is preferred for the purpose of better comparison of our simulation predictions with the KASCADE data. The observed LDD data for electrons and muons are obtained from the KASCADE experiment and their data were reconstructed by the NKG type LDF. On the other hand, the Greisen type LDF is used for estimating the SSP, because the LDF describes lateral muon densities reasonably well in the concerned energy and core distance ranges. We have taken truncated muon sizes for a better comparison with the KASCADE data by counting muons in the core distance interval, 7–200 m. Constraints on the choice of the Moliére radius to 320 or 420 m is made just for the fulfillment of the KASCADE data analysis requirements.

In this chapter we address some aspects of the LAP and SSP arising out of the LDD of EAS electrons and muons, worked out by a detailed simulation study. We check the validity of the scaling behavior of LDD of muons through the LAP and also the SSP as hinted by our earlier works [2]. The present study also correlates these parameters with other EAS observables. Our main focus is to examine the possibility of utilizing observed LAPs estimated from available published KASCADE LDD data of muons, in order to deduce CR mass composition.

The plan of this chapter is the following. In section 4.2 we recall the shape parameters describing the lateral developments of EAS electrons and muons, and definition of the LAP and SSP, is given. Section 4.2 also describes the CORSIKA events used in the procedure of local shape parameter estimation. Section 4.3 is devoted to the data analysis for the estimation of the LAP and SSP. Our results on the primary CR mass sensitivity of these EAS shape parameters are presented and discussed in section 4.4. Section 4.5 summarizes our final conclusions.

4.2 Local age and segmented slope parameters

The shape parameters *viz.* the shower age, or the slope, describing the lateral distributions of shower electrons/photons first came into existence in CR studies through the works of Moliére [4], Rossi and Greisen [5], and lately by Nishimura [6]. During 1956-60, Kamata and Nishimura, and then Greisen independently demonstrated [7, 8] that for hadron initiated EAS, the longitudinal and lateral profiles of electrons/photons can be described by some average overall single shower, assigning some suitable values to the shape parameters.

The average shape of angular distributions or energy distributions of electrons in hadron induced EASs shows the so called universality [9–13]. The universality property is one that limits the stage of shower development in air of every shower, and it is similar (i.e. the same longitudinal shower age, and is ≈ 1) in the vicinity of their shower maxima. This otherwise indicates that the universality behaviour of showers is linked with the stage of the longitudinal shower development or the longitudinal shower age and hence the lateral shower age, s for proton/nuclei induced showers. It is known that the LDD of electrons/muons from any ground based EAS experiment is generally described in terms of shower age or slope parameters.

There has been a numerous number of articles and reviews written by many authors on the concept of shower age/slope and their estimation for several decades ([3, 10, 13–16] and references therein). A more judicious estimation of lateral shower age parameter has been made through LAP in the work [2, 15]. In this work we make an attempt to estimate the both; LAP and SSP particularly from

the LDD of muons, and to derive possible conclusions on the nature of EAS generating primary CR particles.

Observed data of many EAS experiments [15] validated the theoretical prediction by Capdevielle [3] with regard to the erroneous estimation of shower size and the shape parameter using the NKG type LDF. He then resolved the problem in bringing the idea of local shape parameter in place, for the better description of LDD of electrons [2, 3, 16].

According to the concept of local shape parameter, we can now give its analytical expression for an arbitrary LDF in NKG formalism (say, $\mathrm{f(x)}$ with $\mathrm{x} = \frac{\mathrm{r}}{\mathrm{r_D}}$) between two adjacent points $[\mathrm{x_i}, \mathrm{x_j}]$:

$$a(i,j) = \frac{\ln(F_{ij} X_{ij}^{\alpha_1} Y_{ij}^{\alpha_2})}{\ln(X_{ij} Y_{ij})} \tag{4.1}$$

The following substitutions were made in obtaining the local shape parameter: F_{ij} = $f(r_i)$/$f(r_j)$, X_{ij}=r_i/r_j, and Y_{ij}=(x_i+1)/(x_j+1).

More generally, if $x_i \rightarrow x_j$, we will have the local shape parameter $a_{local}(x)$ (or $a_{local}(r)$) at each point. The identification $a_{local}(r) \equiv a_{local}(i,j)$ for $r = \frac{r_i + r_j}{2}$ remains valid for the experimental distributions (taking $F_{ij} = \rho(r_i)/\rho(r_j) \equiv f(r_i)/f(r_j)$).

In cascade theory, the solution of the 3D diffusion equations under some approximations can provide the LDF of cascade particles by the well-known NKG structure function [17], given by

$$\mathrm{f}(r) = \mathrm{C}(s_\perp)(r/r_\mathrm{m})^{s_\perp - 2}(1 + r/r_\mathrm{m})^{s_\perp - 4.5} \ , \tag{4.2}$$

where the normalization factor $\mathrm{C}(s_\perp)$ is given by

$$\mathrm{C}(s_\perp) = \frac{\Gamma(4.5 - s_\perp)}{2\pi\Gamma(s_\perp)\Gamma(4.5 - 2s_\perp)} \ . \tag{4.3}$$

With the help of the structure function $\mathrm{f}(r)$ the electron/muon density ($\rho_{\mathrm{e}/\mu}$) for a constant shape parameter s can be given by

$$\rho_{\mathrm{e}/\mu}(r) = \frac{N_{\mathrm{e}/\mu}}{r_\mathrm{m}^2}\mathrm{f}(r) \ . \tag{4.4}$$

For the reconstruction of experimental LDD of muons, many EAS groups used the structure function proposed by Greisen with different Moliére radii, also called the Greisen radius as expressed in 4.5,

$$f_\mu(r) = \mathrm{A}(r/r_G)^{-\beta}(1 + r/r_G)^{-2.5}, \tag{4.5}$$

with the Greisen radius $r_G = 320$ or 420 m which was amended in various measurements.

For NKG-type LDF, the exponents α_1 and α_2 in the relation 4.1 take values as 4.5 and 2. But for Greisen-type LDF, α_1 and α_2 would take 0 and 2.5 respectively. Moreover, we have modified the denominator in the relation 4.1 by $X_{ji} = X_{ij}^{-1}$ and $Y_{ij} = 1$ while Greisen-type LDF is being considered. The radius parameter $\mathrm{r_D}$ is equal to the Moliére radius $\mathrm{r_m}$ for the NKG LDF, and it is the Greisen radius $\mathrm{r_G}$ for the other case.

For NKG-type LDF i.e. $f_{\mathrm{NKG}}(r)$, $a_{\mathrm{local}}(r)$ was the so called local age parameter (LAP), and denoted by $s_{\mathrm{local}}(r)$ [15, 16]. Similarly for Greisen-type LDF i.e. $f_{\mathrm{Greisen}}(r)$, we denote the shape parameter by $\beta_{\mathrm{ss}}(r)$, is called the SSP.

For the observed LDD data of electrons, the characteristics of LAP as predicted in [18] were reaffirmed by the Akeno [19], KASCADE [3], North Bengal University (NBU) [20] and other experiments [3, 16, 21]. This work gives emphasis on the estimation of the LAP and its mean minimum value in conjunction with the SSP and its mean maximum value especially for the LDD of EAS muons. The general equation 4.1 for estimating the local shape parameter (LAP and SSP), contains only the density and the distance data of an EAS. However, in reference to a real EAS array, these data significantly depend on the accuracy of the density and EAS core measurements, and also the array triggering conditions. Estimated simulated LDD data in the work suit better with the LDD observed data from experiments containing closely packed detectors. We have kept the physical bands of distance; $\Delta_{ij} = \ln r_j - \ln r_i$ equal to ≈ 0.5 on the log scale with increasing the core distance for such types of EAS arrays in the analysis.

A sample of EAS events has been generated by using CORSIKA program version 6.970 [22], which is a full simulation of the shower development initiated by CRs in the earth's atmosphere. The simulated events have been generated by

using the EPOS 1.99 [23] interaction model for the high-energy hadronic interactions, in combination with the UrQMD model [24] for the low-energy hadronic interactions. A smaller sample of the MC events has also been generated by combining the high-energy hadronic interaction model QGSJet01.c [25] with the same UrQMD model for the low-energy hadronic interactions. The electromagnetic interactions of the EAS is implemented by means of the EGS4 [26] program package.

Only proton and iron showers have been generated for obtaining an indication on the probable mass composition of PCRs from KASCADE data. The simulated events in the primary energy range 10^{14} eV to 3×10^{15} eV have been generated according to the following distribution, given by

$$N(E)dE = N_0 E^{-\gamma} dE. \tag{4.6}$$

The spectral index in the above primary energy range has been taken as $\gamma = 2.7$ and a total of about 2×10^5 showers have been generated. Beyond this energy range, about 2500 events have been generated with $\gamma = 3.1$. Showers have been generated at the KASCADE [27] altitude by setting kinetic energy cut-offs for different secondary particles in the CORSIKA steering file, restricting zenith angle (Θ) in the range $0^o - 18^o$.

4.3 Shower data analysis: Estimation of the LAP and SSP

We have computed the LAP for the LDD of electrons and muons for each simulated event independently by using equation 4.1. The NKG-type LDF was used for $\mathrm{f}(r)$ in the equation. The Moliére radius was taken as 89 m for electrons while for muons, r_{m} took values as 320 m and 420 m in two different cases, as used in the analysis of KASCADE data. For computing the SSP, the Greisen-type LDF was chosen with the Greisen radius 320 m and 420 m independently. The estimations of the LAP and the SSP are affected by an average statistical error of the order of $\pm 5\%$ for $7\ \mathrm{m} < \mathrm{r} \leq 300$ m around the *knee* energies. However, for $\mathrm{r} < 7$ m and $\mathrm{r} > 300$ m the error for the LAP and SSP may rise up to about $\pm 10\%$. The sources of statistical error are due to mainly in the fluctuations in electron/muon

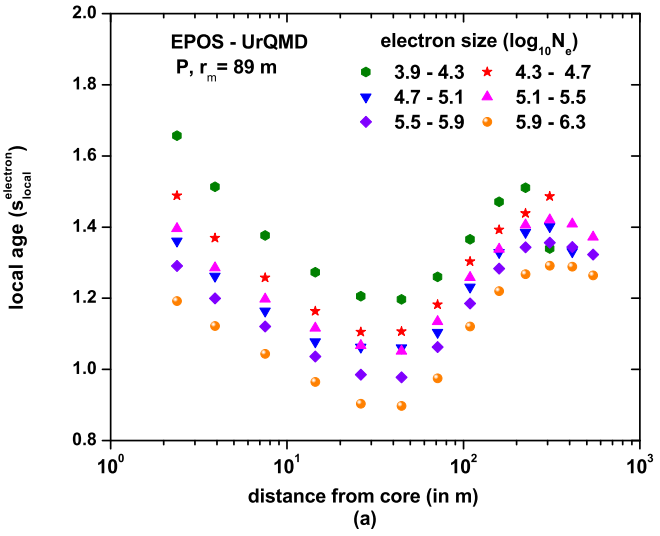
EPOS - UrQMD
P, r_m = 89 m
electron size (log10Ne)
3.9 - 4.3
4.3 - 4.7
4.7 - 5.1
5.1 - 5.5
5.5 - 5.9
5.9 - 6.3
local age (s^electron_local)
distance from core (in m)

(a)

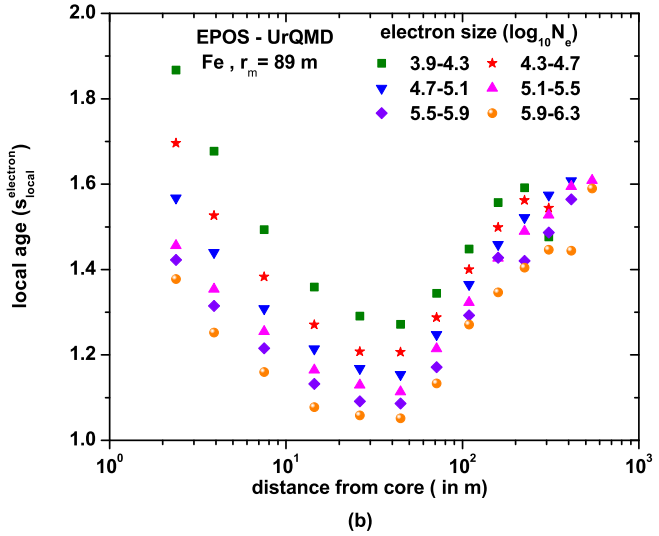
EPOS - UrQMD
Fe , r_m = 89 m
electron size (log10Ne)
3.9-4.3
4.3-4.7
4.7-5.1
5.1-5.5
5.5-5.9
5.9-6.3
local age (s^electron_local)
distance from core (in m)

(b)

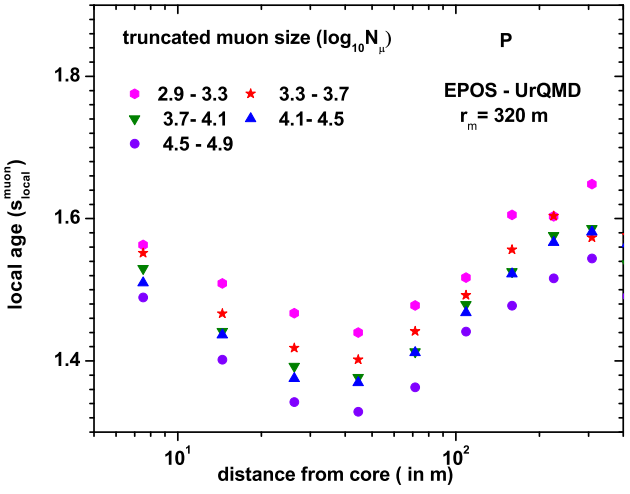
truncated muon size (log10Nμ)
P
2.9 - 3.3
3.3 - 3.7
3.7- 4.1
4.1- 4.5
4.5 - 4.9
EPOS - UrQMD
r_m = 320 m
local age (s^muon_local)
distance from core (in m)

(c)

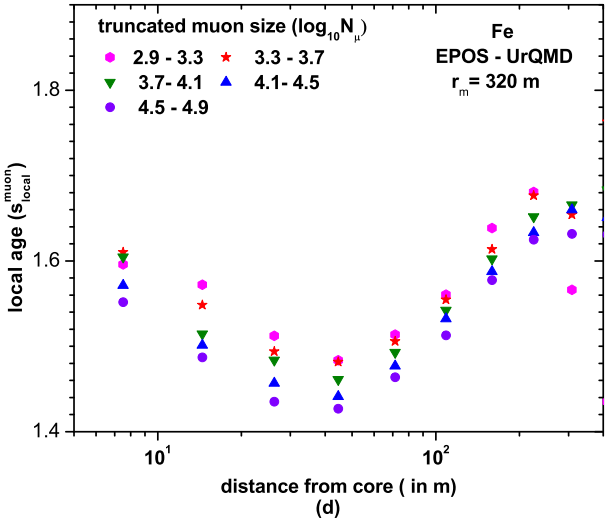

FIGURE 4.1: Variation of the LAP with radial distance at the KASCADE site for different shower (or electron) size and muon size (truncated) intervals. Figure (a) and (b) for proton and iron showers using simulated LDD data of electrons. Figure (c) and (d) show the similar variations but with the LDD data of muons.

densities and the uncertainties in core distance measurement. Simulated data provide very accurate position of each EAS particle, and hence the core distance estimation contributes very small errors to the estimations of the LAP and SSP. For controlling the statistical fluctuations over the estimations in electron/muon densities at different distance bands, a reasonable sample size of EAS events need to be considered. It is noticed that the LAP estimated from KASCADE data experiencing higher fluctuations, compared to simulation results. The variation of the LAP and SSP with radial distance from the EAS core is a fundamental study of this chapter. The radial variation of the LAP, especially for the LDD of electrons, was studied extensively in some earlier works [2, 14, 29]. Here we have focused particularly on the LDD of muons for studying the radial dependence of the LAP and also the SSP, and hence to explore the primary mass sensitivity of the LAP from the KASCADE muon data.

Among the ongoing experiments, GRAPES-3 may successfully implement the proposed method for estimating the LAP and the SSP by using their muon data. Being a closely packed air shower array of scintillation detectors, the uncertainty arises from the radial distance (or the core position) measurement would be small. On the other hand, the expanded size of its muon detector ($\approx 1120\ \mathrm{m}^2$) may provide more accurate measurements for muon densities around the *knee*

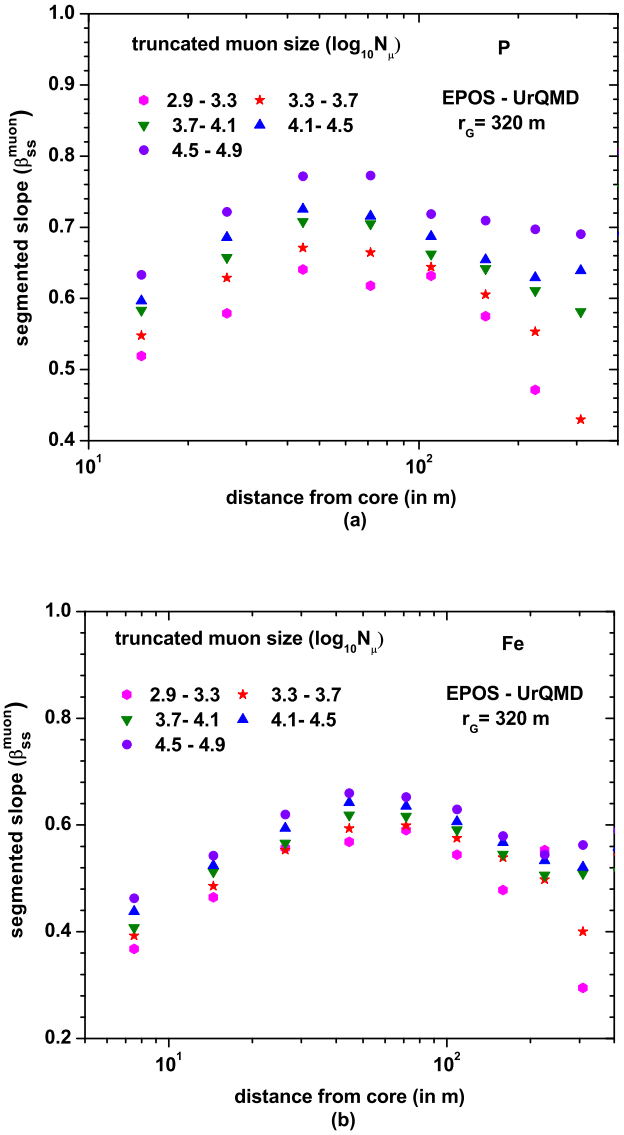

FIGURE 4.2: Variation of the SSP with radial distance at the KASCADE site for different muon size intervals. Figure (a) and (b), for proton and iron showers using simulated LDD data of muons only.

energy and beyond. The variations of $s_{\rm local}(r)$ and $\beta_{\rm ss}(r)$ with r at KASCADE location around the *knee* energy and beyond are shown in Fig. 4.1, for nearly vertical showers initiated by protons and iron nuclei. Figs. 4.1a and 4.1b represent $s_{\rm local}(r)$ versus r variations for the LDD of electrons, initiated by proton and iron showers. Similar plots for the LDD of muons are shown in Fig. 4.1c and 4.1d. On the other hand, in Fig. 4.2a and 4.2b, such type of studies are depicted for the parameter $\beta_{\rm ss}(r)$ using the LDD of muons only. The findings in Fig. 4.1a and 4.1b for the LDD data of electrons reaffirm the well established fact related to the radial variation of $s_{\rm local}(r)$, that found in previous studies [2, 7]. It should

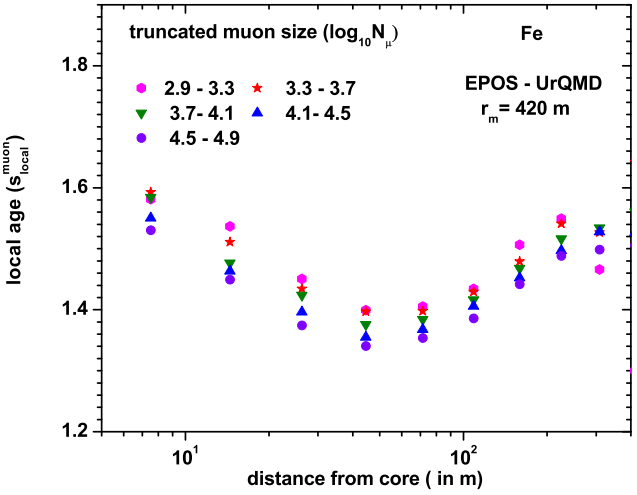
truncated muon size ($\log_{10}N_\mu$)
Fe
EPOS - UrQMD
r_m= 420 m
2.9 - 3.3
3.3 - 3.7
3.7- 4.1
4.1- 4.5
4.5 - 4.9
local age (s^{muon}_{local})
distance from core (in m)

(a)

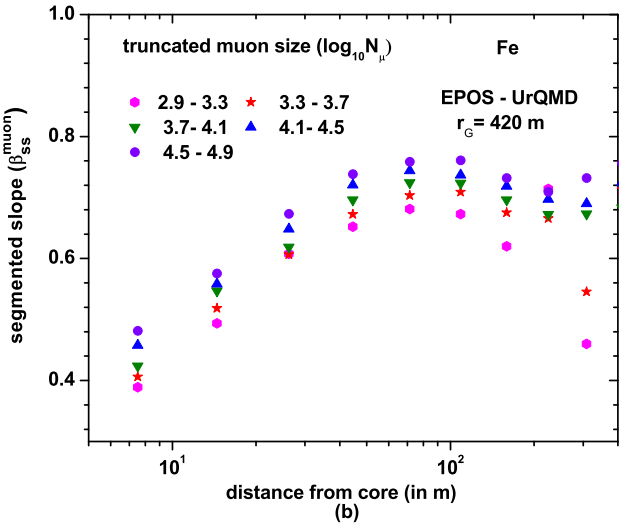
truncated muon size ($\log_{10}N_\mu$)
Fe
EPOS - UrQMD
r_G= 420 m
2.9 - 3.3
3.3 - 3.7
3.7- 4.1
4.1- 4.5
4.5 - 4.9
segmented slope (β^{muon}_{ss})
distance from core (in m)

(b)

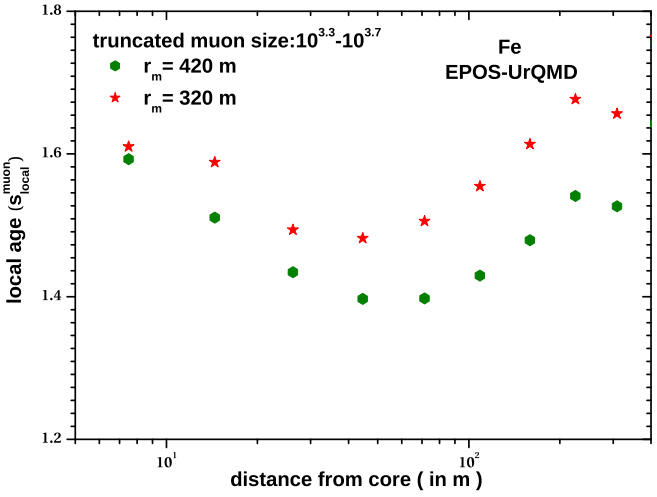
truncated muon size:$10^{3.3}$-$10^{3.7}$
Fe
EPOS-UrQMD
r_m= 420 m
r_m= 320 m
local age (s^{muon}_{local})
distance from core (in m)

(c)

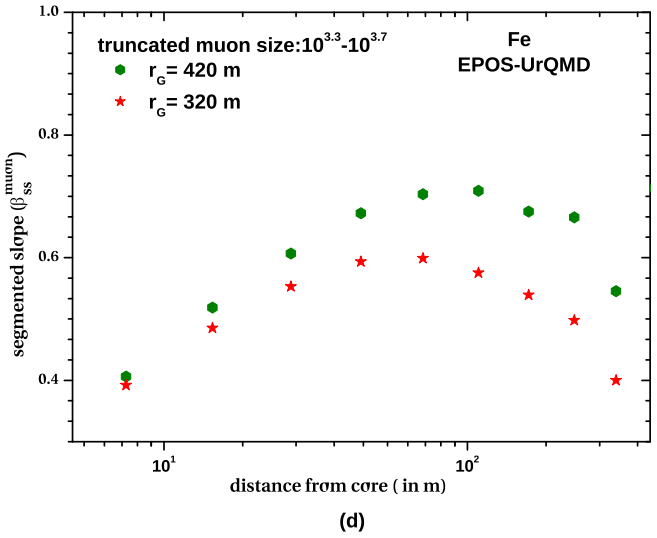

FIGURE 4.3: Variations of the LAP and SSP with radial distance at the KASCADE site for different muon size intervals, for simulated iron showers. Figure (a) and (b) show the radial variation for the LAP and SSP independently with the Moliére radius - 420 m. Figure (c) and (d) show the similar variations for the LAP and SSP independently with two different values of the Moliére and Greisen radii. EPOS model is used for high energy hadronic interactions.

be however mentioned that such type of variations of $s_{\rm local}(r)$ with r in the case of LDD of muons (Fig. 4.1c and 4.1d) are reported first time in this work. Interestingly the shapes of the radial variation versus local age curves estimated from the LDD of muons and electrons look almost similar in nature. Furthermore, some previous studies [2] observed that the shape of these variations are independent of the energy of the EAS initiating particles and also the observation level. Here we noticed that the above features of the local age do not change even though electrons and muons in an EAS experience different attenuation and geomagnetic influence during their advancement in the atmosphere [30]. In Fig. 4.2a and 4.2b, we have noticed an opposite trend in the $\beta_{\rm ss}(r)$ parameter relative to $s_{\rm local}(r)$. It can be concluded that the local age and the segmented slope (or the LDD of electrons and muons) exhibit some sort of scaling behavior while varied as a function of the core distance. To examine the effect of the Moliére radius/-Greisen radius we take the Moliére radius as $\rm r_m = 320$ m, $\rm r_m = 420$ m (that was used by the KASCADE experiment), with EPOS as the high-energy hadronic interaction model. For this value of the $\rm r_m$, we have obtained little lower values for $s_{\rm local}(r)$ corresponding to the previous set of radial distances. But, for the above change in $\rm r_G$, the $\beta_{\rm ss}(r)$ parameter receives little higher values instead. Such a

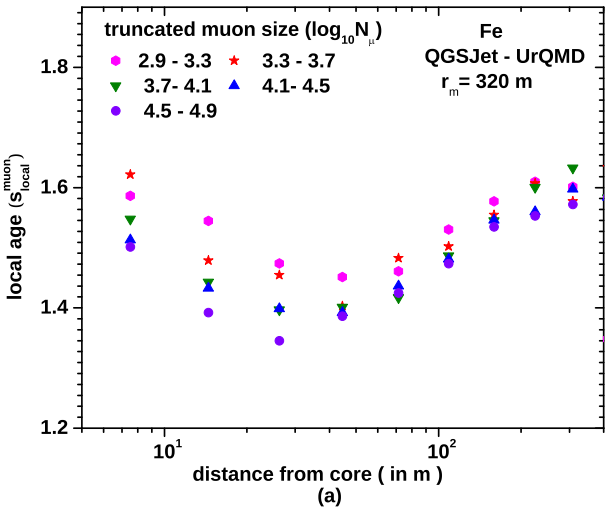
truncated muon size ($\log_{10}N_\mu$)
2.9 - 3.3
3.3 - 3.7
3.7- 4.1
4.1- 4.5
4.5 - 4.9
Fe
QGSJet - UrQMD
r_m= 320 m
local age (s^{muon}_{local})
distance from core (in m)

(a)

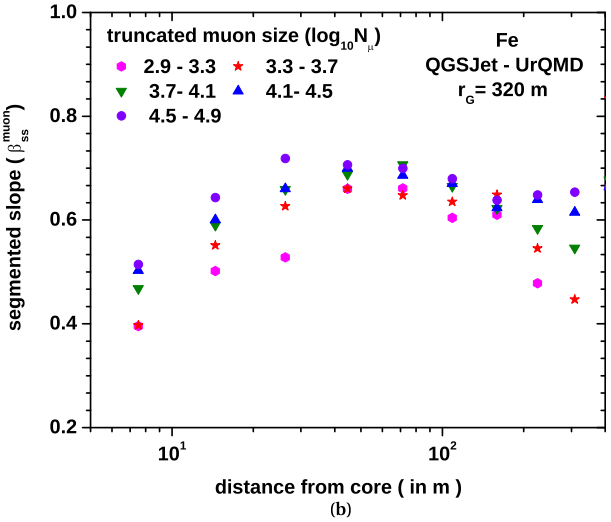
truncated muon size ($\log_{10}N_\mu$)
2.9 - 3.3
3.3 - 3.7
3.7- 4.1
4.1- 4.5
4.5 - 4.9
Fe
QGSJet - UrQMD
r_G= 320 m
segmented slope (β^{muon}_{ss})
distance from core (in m)

(b)

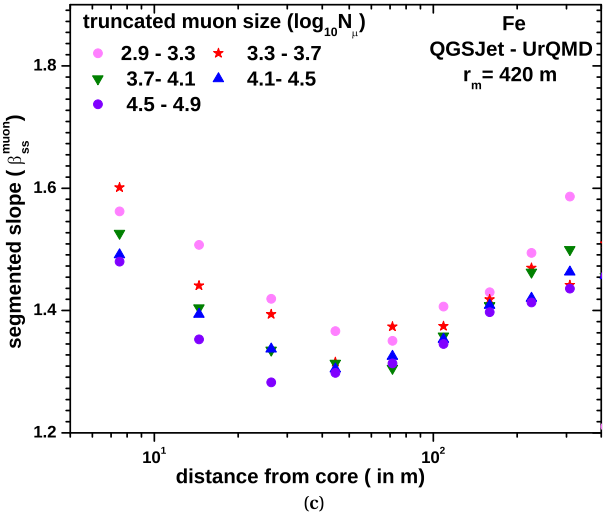
truncated muon size ($\log_{10}N_\mu$)
2.9 - 3.3
3.3 - 3.7
3.7- 4.1
4.1- 4.5
4.5 - 4.9
Fe
QGSJet - UrQMD
r_m= 420 m
segmented slope (β^{muon}_{ss})
distance from core (in m)

(c)

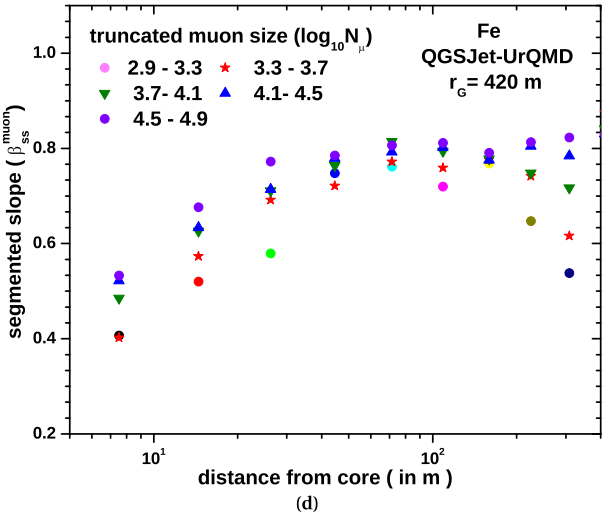

FIGURE 4.4: Variations of the LAP and SSP with radial distance at the KASCADE site for different muon size intervals, for simulated iron showers. Figure (a) and (b) show the radial variation for the LAP and SSP independently with the Moliére radius - 320 m. Figure (c) and (d) show the similar variations for the LAP and SSP independently with the Moliére/Greisen radius - 420 m each. QGSJet model is used for high energy hadronic interactions.

study is shown in Figs. 4.3a, 4.3b,4.3c and 4.3d for Fe initiated showers with EPOS model. Here, we have noticed that the Moliére radius/Greisen radius has just changed the scale of $s_{\rm local}(r)$ and/or $\beta_{\rm ss}(r)$ but retaining the shape of the radial variation unchanged. In Fig. 4.4a, 4.4b, 4.4c and 4.4d, we have presented results on the radial dependence of these parameters taking the QGSJet v.1c model for high energy hadronic interaction.

If attempts are made to explore the possible causes for such a behavior of the $s_{\rm local}(r)$ or $\beta_{\rm ss}(r)$ or the LDD of electrons/muons, we should at least look at the EGS4 and NKG options closely. In simulations, particularly at the last stage of the cascade development, the generation and absorption of the electromagnetic components are the outcome of different processes/mechanisms implemented in EGS4 package. On the other hand, the LDD data of electrons/muons resulted from the several mechanisms (Moller, Bhaba sattering, positron annihilation etc.) in EGS4 option, were used to estimate the $s_{\rm local}(r)$ or $\beta_{\rm ss}(r)$ parameters. These parameters were defined in terms of the NKG or Greisen functions (equation 4.1), that could be obtained from solutions of the cascade equations applying several approximations. From some previous studies [3, 16, 21], it was learned that the nature of $s_{\rm local}(r)$ arises due to the description of EGS4/observed data by

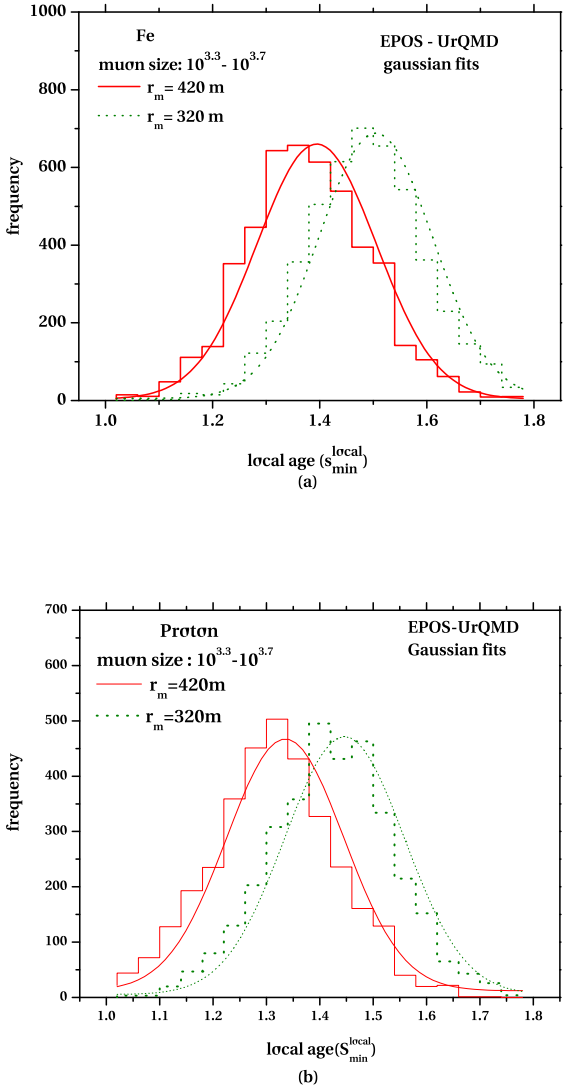

FIGURE 4.5: Distribution of the mean minimum LAP from simulated muon LDD data initiated by iron primaries for two different Moliére radii. Figure (a) - iron; Figure (b) - proton.

the approximate LDFs (e.g. NKG), called shower reconstruction, for obtaining the required EAS parameters. In the NKG-type LDF, the azimuthal distribution of EAS electrons/muons is considered symmetric. But, it is inevitable that the azimuthal distribution of EAS particles is asymmetric.

The scale distance such as the Moliére/Greisen radius used in the LDF functions may lead to determine the shape of the $s_{\rm local}(r)$ or $\beta_{\rm ss}(r)$ versus r curves [2]. The above idea of $\rm r_m$ dependent $s_{\rm local}(r)$ has been corroborated from the frequency distribution of the minimum values of $s_{\rm local}(r)$ (obtained from r versus $s_{\rm local}(r)$ plots for two different Moliére radii), which are shown in Fig. 4.5a and 4.5b.

4.4 Results concerning cosmic ray composition

The present analysis is based on the shape of the simulated/observed LDF derived from electrons/muons LDD data. To probe the CR mass sensitivity associated with the slope/shape, particularly for muons, we studied some important characteristics of the LAP and the SSP. To assign a single age to every shower, we have first attempted to estimate the minimum value of the local age within a suitably chosen electron size/muon size interval by averaging its values exactly at the radial distance 44 m. Applying the same procedure, we have computed the mean maximum segmented slope exactly at the radial distance 71 m.

In Table 4.1 and Table 4.2, we have presented our results by applying the above technique for the mean value of the minimum local age parameter (s_{min}^{local}) corresponding to mean electron and muon sizes (truncated). For the mean value of the maximum segmented slope parameter (β_{max}^{ss}) our findings are given in Table 4.3 and Table 4.4 respectively.

TABLE 4.1: Analysis showing the dependence of mean minimum local age parameter with electron size at 44 m from shower core.

Moliére radius = 320 m Electron size (N_e)	Mean local age (s_{min}^{local}) Iron	Uncertainty	Mean local age(s_{min}^{local}) Proton	Uncertainty
$10^{3.9} - 10^{4.3}$	1.488	$\pm 9.0\%$	1.472	$\pm 10.5\%$
$10^{4.3} - 10^{4.7}$	1.476	$\pm 7.0\%$	1.437	$\pm 9.6\%$
$10^{4.7} - 10^{5.1}$	1.460	$\pm 5.0\%$	1.403	$\pm 8.4\%$
$10^{5.1} - 10^{5.5}$	1.445	$\pm 4.0\%$	1.360	$\pm 7.1\%$
$10^{5.5} - 10^{5.9}$	1.437	$\pm 2.7\%$	1.347	$\pm 6.3\%$
$10^{5.9} - 10^{6.3}$	1.417	$\pm 2.5\%$	1.334	$\pm 5.8\%$
Moliére radius = 420 m				
$10^{3.9} - 10^{4.3}$	1.403	$\pm 10.0\%$	1.386	$\pm 11.0\%$
$10^{4.3} - 10^{4.7}$	1.392	$\pm 8.0\%$	1.351	$\pm 10.0\%$
$10^{4.7} - 10^{5.1}$	1.375	$\pm 6.0\%$	1.316	$\pm 9.0\%$
$10^{5.1} - 10^{5.5}$	1.359	$\pm 4.3\%$	1.273	$\pm 7.7\%$
$10^{5.5} - 10^{5.9}$	1.351	$\pm 3.0\%$	1.260	$\pm 6.8\%$
$10^{5.9} - 10^{6.3}$	1.330	$\pm 2.72\%$	1.244	$\pm 6.4\%$

The results presented in the above tables reveal that the magnitudes of s_{min}^{local} and β_{max}^{ss} have maintained a good contrast between proton and iron primaries but their uncertainties particularly for β_{max}^{ss} sometimes exceed even the limit $\pm 20\%$. Hence it would be more judicious to take a mean minimum value of s_{local} evaluated from few local ages at the radial distance, about 44 m and also a mean maximum value of few β_{ss} at the radial distance, about 71 m instead. We have applied this method in estimating the mean s_{min}^{local} and β_{max}^{ss} for the measurement of CR mass

TABLE 4.2: Analysis showing the dependence of mean local age(s_{min}^{local}) with truncated muon size at 44 m from shower core.

Moliére radius = 320 m Muon size (N_μ)	Mean local age (s_{min}^{local}) Iron	Uncertainty	Mean local age (s_{min}^{local}) Proton	Uncertainty
$10^{2.9} - 10^{3.3}$	1.484	$\pm 8.7\%$	1.417	$\pm 9.7\%$
$10^{3.3} - 10^{3.7}$	1.473	$\pm 6.5\%$	1.391	$\pm 7.2\%$
$10^{3.7} - 10^{4.1}$	1.451	$\pm 4.4\%$	1.371	$\pm 5.2\%$
$10^{4.1} - 10^{4.5}$	1.435	$\pm 2.6\%$	1.361	$\pm 4.4\%$
$10^{4.5} - 10^{4.9}$	1.415	$\pm 2.1\%$	1.290	$\pm 8.0\%$
Moliére radius = 420 m				
$10^{2.9} - 10^{3.3}$	1.399	$\pm 9.5\%$	1.331	$\pm 10.6\%$
$10^{3.3} - 10^{3.7}$	1.388	$\pm 6.7\%$	1.304	$\pm 7.8\%$
$10^{3.7} - 10^{4.1}$	1.365	$\pm 4.8\%$	1.283	$\pm 5.7\%$
$10^{4.1} - 10^{4.5}$	1.349	$\pm 2.9\%$	1.273	$\pm 4.8\%$
$10^{4.5} - 10^{4.9}$	1.328	$\pm 2.3\%$	1.199	$\pm 8.7\%$

TABLE 4.3: Analysis showing the dependence of mean segmented slope parameter (β_{max}^{ss}) with electron size at 71 m from shower core.

Greisen radius = 320 m Electron size (N_e)	Mean segmented slope parameter (β_{max}^{ss}) Iron	Uncertainty	Mean segmented slope parameter(β_{max}^{ss}) Proton	Uncertainty
$10^{3.9} - 10^{4.3}$	0.592	$\pm 24.0\%$	0.594	$\pm 28.0\%$
$10^{4.3} - 10^{4.7}$	0.611	$\pm 19.4\%$	0.637	$\pm 22.5\%$
$10^{4.7} - 10^{5.1}$	0.622	$\pm 14.4\%$	0.676	$\pm 17.7\%$
$10^{5.1} - 10^{5.5}$	0.641	$\pm 9.9\%$	0.707	$\pm 14.0\%$
$10^{5.5} - 10^{5.9}$	0.645	$\pm 9.7\%$	0.727	$\pm 10.9\%$
$10^{5.9} - 10^{6.3}$	0.662	$\pm 6.2\%$	0.752	$\pm 9.3\%$
Greisen radius=420 m				
$10^{3.9} - 10^{4.3}$	0.696	$\pm 19.7\%$	0.708	$\pm 20.0\%$
$10^{4.3} - 10^{4.7}$	0.716	$\pm 16.0\%$	0.741	$\pm 17.6\%$
$10^{4.7} - 10^{5.1}$	0.728	$\pm 12.0\%$	0.775	$\pm 13.7\%$
$10^{5.1} - 10^{5.5}$	0.748	$\pm 8.8\%$	0.801	$\pm 11.4\%$
$10^{5.5} - 10^{5.9}$	0.755	$\pm 6.3\%$	0.817	$\pm 8.4\%$
$10^{5.9} - 10^{6.3}$	0.768	$\pm 5.4\%$	0.842	$\pm 6.7\%$

TABLE 4.4: Analysis showing the dependence of mean segmented slope parameter (β_{max}^{ss}) with truncated muon size at 71 m from shower core

Greisen radius = 320 m Muon size(N_μ)	Mean segmented slope parameter(β_{max}^{ss}) Iron	Uncertainty	Mean segmented slope parameter(β_{max}^{ss}) Proton	Uncertainty
$10^{2.9} - 10^{3.3}$	0.598	$\pm 23.0\%$	0.659	$\pm 21.6\%$
$10^{3.3} - 10^{3.7}$	0.612	$\pm 17.0\%$	0.686	$\pm 15.0\%$
$10^{3.7} - 10^{4.1}$	0.632	$\pm 10.9\%$	0.707	$\pm 10.6\%$
$10^{4.1} - 10^{4.5}$	0.645	$\pm 8.8\%$	0.738	$\pm 8.3\%$
$10^{4.5} - 10^{4.9}$	0.661	$\pm 4.7\%$	0.750	$\pm 3.2\%$
Greisen radius = 420 m				
$10^{2.9} - 10^{3.3}$	0.703	$\pm 19.0\%$	0.758	$\pm 16.7\%$
$10^{3.3} - 10^{3.7}$	0.717	$\pm 14.7\%$	0.782	$\pm 12.5\%$
$10^{3.7} - 10^{4.1}$	0.738	$\pm 9.5\%$	0.804	$\pm 8.6\%$
$10^{4.1} - 10^{4.5}$	0.754	$\pm 5.7\%$	0.835	$\pm 6.7\%$
$10^{4.5} - 10^{4.9}$	0.767	$\pm 4.0\%$	0.856	$\pm 2.9\%$

composition. The uncertainties of these observables are now reduced remarkably, and they remain within $\pm 10\%$.

4.4.1 Variation of the minimum local age with shower size and muon size

We have plotted the mean minimum local age against mean shower size, obtained from simulated electron LDD data for proton and iron initiated showers at the KASCADE level in Fig. 4.6a. In order to judge the effect of the high-energy hadronic interaction model on the above result, if any, we have plotted the above variation for the QGSJet model in Fig. 4.6b. In the above plots, the corresponding observed results extracted from the KASCADE data [27, 28] are also presented. These two plots strongly favour the idea that KASCADE data indicate a gradual change in the CR mass composition across the *knee* from a lighter towards a heavier, as the shower size/primary energy increases. Using the N_e-N_μ variations the KASCADE experiment also arrived at the similar inference on the CR mass composition across the *knee*. We have found a little better results with the interaction model QGSJet over the EPOS 1.99 here.

The variation of the mean minimum LAP with mean muon size, obtained from simulated muon LDD data for proton and iron initiated showers, using the EPOS interaction model at the KASCADE level for two different Moliére radii are shown in Fig. 4.7a and 4.7c. The observed data points for the mean minimum LAPs, that have been included into the plots, estimated from extracted KASCADE muon LDD [29]. In Fig. 4.7b, we have studied the same variation but with the high-energy hadronic interaction model QGSJet. It has been noticed here that the mean minimum LAP obtained from simul ated muon LDD data decreases slowly with mean muon size compared to similar curves found in case of the LDD of electrons. This might be due to a relatively flatter density profile for muons compared to the case for electrons, which is a generic feature of an EAS.It is revealed that the KASCADE muon data also indicates a heavier domination with increasing muon size/energy across the *knee*. No appreciable difference is found in the Fig. 4.7a from Fig. 4.7b due to hadronic interaction model QGSJet.

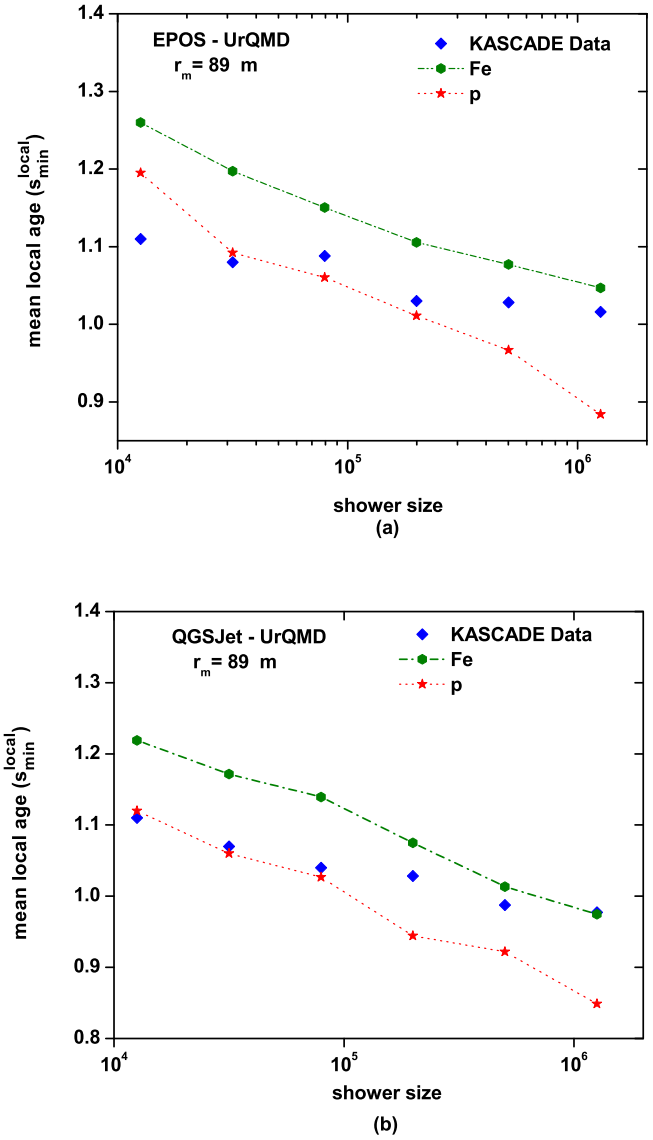

FIGURE 4.6: Variation of the mean minimum LAP with shower size for proton and iron primaries for (a) EPOS and (b) QGSJet models at the KASCADE site along with the experimental data. The lines are drawn for the purpose of guidance to our eyes.

4.4.2 Variation of the maximum segmented slope with muon size

The variation of the mean maximum segmented slope with muon size for proton and iron initiated showers is studied using simulated LDD data only. As mentioned above that the SSP has been estimated using the equation 4.1 with the Greisen type LDF. There was no observed muon LDD data available in published papers fitted by the Greisen function from the KASCADE group to estimate the SSP. In Fig. 4.8a, 4.8b and 4.8c, our simulated results on the variation between the mean maximum segmented slope and the muon size are depicted. All these

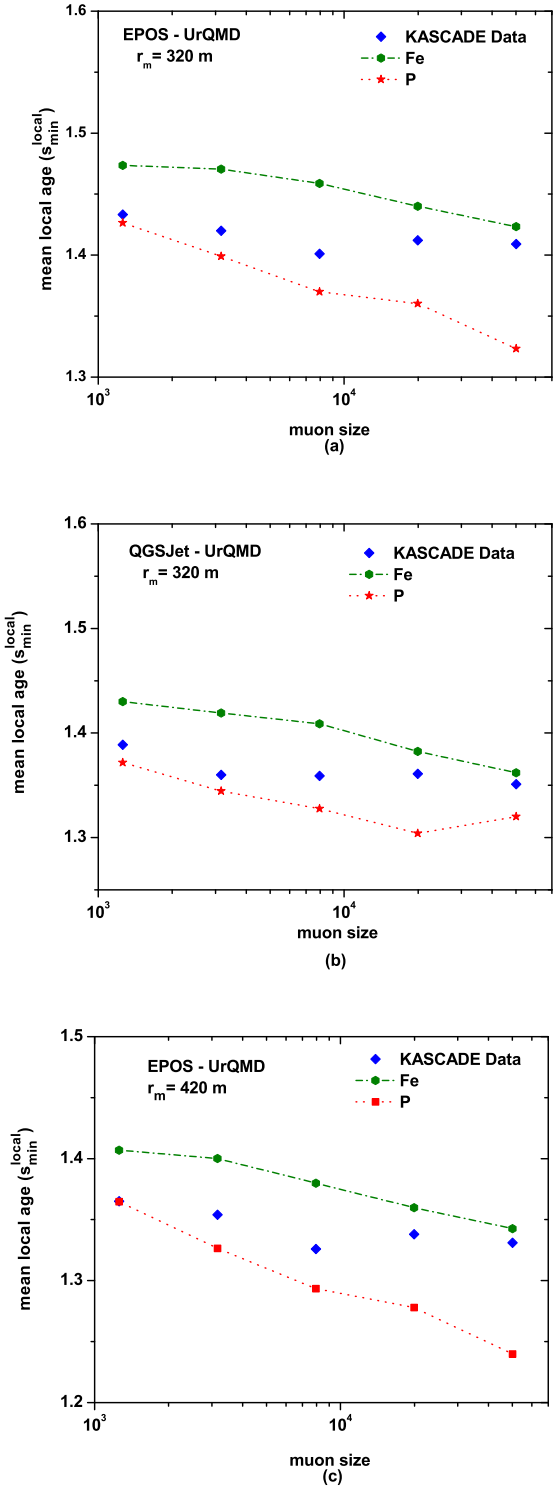

FIGURE 4.7: Variation of the mean minimum LAP with muon size for proton and iron primaries for (a) EPOS and (b) QGSJet models taking $r_m = 320$ m at the KASCADE site along with the experimental data. Figure (c) shows the similar variation but with $r_m = 420$ m. The lines are drawn for the purpose of guidance to our eyes.

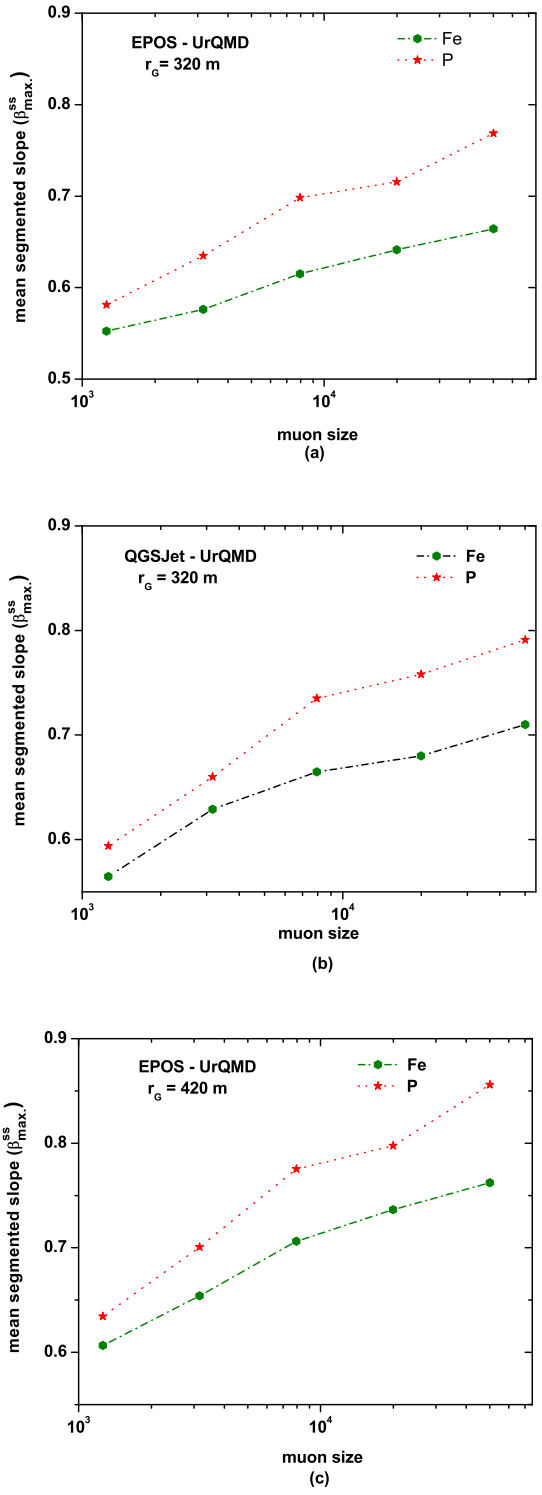

FIGURE 4.8: Variation of the mean maximum SSP with muon size for proton and iron primaries for (a) EPOS and (b) QGSJet models taking $r_G = 320$ m at the KASCADE site. Figure (c) shows the similar variation but with $r_G = 420$ m. The lines are drawn for the purpose of guidance to our eyes.

variations follow a completely opposite trend compared to the variations seen in Fig. 4.7a, 4.7b and 4.7c. We have seen a marginal hadronic interaction model dependence of these variations. Even for different Greisen radii, these results seem almost unaltered. It is expected that if observed LDD data (with or without fitted by the Greisen-type LDF) for muons are available, the mean maximum SSP might be able to estimate the CR mass composition.

In the present analysis, the errors in estimating the mean minimum LAP in the shower size interval 10^4–10^6 result in the range $\pm(0.03$–$0.05)$, irrespective of the high-energy hadronic interaction model. In the truncated muon size interval i.e. 10^3–5×10^4, this analysis yielded comparable errors of above magnitudes in estimating the mean minimum local age and the mean maximum segmented slope. However, the uncertainty in estimating the local age from KASCADE electron and muon data has reached up to ± 0.1 or even little beyond.

4.5 Conclusions

In the present analysis, attempts have been made to estimate the mass composition of primary CRs across the *knee* on the basis of the characteristic feature of the LAP/SSP versus the radial distance curves. The overall configurations of the $s_{\rm local}(r)$ versus r curves are found almost independent to electron and muon distributions respectively. These characteristic variations in the LAP appear as a basic feature among different secondary components of a shower. The muonic cascades also exhibit such a universal behaviour in terms of the SSP as well.

The characteristic features of the LAP and SSP allow a more accurate estimation of the shower age and the slope of a shower. We have found a strong dependence of the LAP and SSP on the radial distance. In experimental LDD data, it was noticed by many that the radius of the shower disc may vary, from one event to another. Again the LAP or SSP in the radial distance limits $\mathrm{r} < 7$ m (due to large fluctuations in LDD data) or/and $\mathrm{r} > 100$ m (due to rapid fall in densities of electrons/muons) receive more uncertainty. A more practical consideration could be to take the mean minimum LAP and the mean maximum SSP at intermediate distances about 44 m and 71 m respectively. At these particular distances

some sort of consistency is found in the LAP and SSP from one event to another irrespective of EAS initiating particles or shower sizes/muon sizes.

The scale distance such as the Moliére/Greisen radius used in the LDF functions may lead to determine the shape of the $s_{\rm local}(r)$ or $\beta_{\rm ss}(r)$ versus r curves. The frequency distributions of the minimum values of $s_{\rm local}(r)$ for two different Moliére radii possess different mean values. This suggests that the scale distance regulates the shape of the $s_{\rm local}(r)$ or $\beta_{\rm ss}(r)$ versus r curves on a statistical basis.

The KASCADE experimental data in the Figs. 4.6 and 4.7 indicate that the mass composition follows a gradual change from predominantly lighter (proton-dominated) to heavier (iron-dominated) nuclei with the increase of shower/muon size. This above feature supports the results obtained from the study of the $N_{\rm e}$–N_{μ} variations in the KASCADE experiment. The variations in Fig. 4.7a and 4.7b with muons are flatter than that in Fig. 4.6a and 4.6b with electrons, as per expectation. Our results are found almost independent to high-energy hadronic interaction models as well.

The mean maximum SSP versus muon size variations shown in Fig. 4.8 might give an interesting task to apply it for mass composition study from the KASCADE or other existing or upcoming muon installations.

Bibliography

[1] J. N. Capdevielle and J. Procureur, *Proc. 18th ICRC.*, Bangalore, **11**, 307 (1983).

[2] R. K. Dey, A. Bhadra and J. N. Capdevielle, *J. Phys. G:Nucl. Part. Phys.*, **39**, 085201 (2012).

[3] J. N. Capdevielle and J. Gawin, *J. of Physics G.*, **8**, 1317 (1982).

[4] G. Moli‘ere,: Cosmic Radiation, W. Heisenberg, ed., Dover Publications, New York, 1st ed., (1946).

[5] B. Rossi and K Greisen, *Rev. Mod. Phys.*, **13**, 240 (1941).

[6] J. Nishimura, and K. Kamata, *Progr. Theor. Phys.*, **5**, 899 (1950).

[7] K. Kamata and J. Nishimura, *Prog. Theor. Phys. Suppl.*, **6**, 93 (1958).

[8] K. Greisen, *Ann. Rev. of Nucl. and Part. Science.*, **10**, 63 (1960).

[9] M. Giller, A. Kacperczyk, J. Malinowski, G. TkaczykWandWieczorek, *J. Phys. G: Nucl. Part. Phys.*, **31**, 947 (2005).
F. Nerling, J. Blumer, R. Engel and M. Risse, *Astropart. Phys.*, **24**, 421 (2006).

[10] P. Lipari, *Phys. Rev. D* **79**, 063001 (2009).

[11] S. Lafebre, R. Engel, H. Falcke, J. Hoerandel, T. Huege, J. Kuijpers and R. Ulrich, *Astropart. Phys.*, **31**, 243 (2009).

[12] F. Schmidt, M. Ave, L. Cazon and A. Chou, *Astropart. Phys.*, **29**, 355 (2008).
D. Gora et al., *Astropart. Phys.*, **24**, 484 (2006).

[13] R. K. Dey and S. Dam, *Eur. Phys.J. Plus*, **131**, 402 (2016).

[14] J. N. Capdevielle, J. Cohen, *J. Phys. G: Nucl. Part. Phys.*, **31**, 507 (2005).

[15] J. N. Capdevielle and J. Procureur, *Proc. 18th ICRC.*, Bangalore, **11**, 307 (1983).

[16] M.F. Bourdeau, J.N. Capdevielle and J. Procureur, *J. Phys.G.*, **6**, 901 (1980).

[17] K. Greisen, *Prog. in Cosmic Ray Physics*, North Holland, Co., Amsterdam, **3** 1 (1956).

[18] J.N. Capdevielle et al., *J. Phys. G: Nucl. Part. Phys.*, **31**, 507 (2005).

[19] M. Nagano et al., *J. Phys. Soc.*, Japan **53**, 1667 (1984); M. Nagano et al., *J. Phys. G.*, **10**, 1295–1310 (1984).

[20] S. Sanyal et al., *Aust. J. Phys.*, **46**, 589 (1993).

[21] J. N. Capdevielle and P. Gabinski, *J. Phys. G.:Nucl. Part. Phys.*, **16**, 769 (1990).

[22] D. Heck, J. Knapp, J. N. Capdevielle, G. Schatz and T. Thouw, FZKA report-6019 ed. FZK *The CORSIKA Air Shower Simulation Program*, Karlsruhe (1998).

[23] K. Werner, et al., *Phys. Rev. C*, **74**, 044902 (2006).

[24] M. Bleicher, et al., *J. Phys. G: Nucl. Part. Phys.*, **25**, 1859 (1999).

[25] N. N. Kalmykov, S. S. Ostapchenko and A. I. Pavlov, *Nucl. Phys. (Proc. Suppl.)*, B **52** 17 (1997).

[26] W. R. Nelson, H. Hiramaya, D. W. O. Rogers, Report SLAC 265, (1985).

[27] W. D. Apel et al., *Astropart. Phys.*, **24**, 467 (2006).

[28] A. Bhadra et al., *Nucl. Instrum. Methods*, A **414**, 233 (1998).

[29] T. Antoni et al., *Astropart. Phys.*, **14**, 245 (2001).

[30] R. K. Dey and S. Dam, *Exp Astron*, **43**:75–98 (2017)